THE JOURNAL OF BIOLOGICAL CHEMISTRY
Vol. 279, No. 50, Issue of December 10, pp. 52227–52237, 2004
Printed in U.S.A.

Proton-assisted Two-electron Transfer in Natural Variants of Tetraheme Cytochromes from *Desulfomicrobium* Sp.*

Received for publication, August 2, 2004, and in revised form, September 17, 2004
Published, JBC Papers in Press, September 28, 2004, DOI 10.1074/jbc.M408763200

Ilídio J. Correia‡§, Catarina M. Paquete‡, Ana Coelho‡¶, Claudia C. Almeida‡, Teresa Catarino‡‖, Ricardo O. Louro‡, Carlos Frazão‡, Lígia M. Saraiva‡, Maria Arménia Carrondo‡, David L. Turner‡, and António V. Xavier‡ ‡‡**

*From the ‡Instituto de Tecnologia Química e Biológica, Universidade Nova de Lisboa, Rua da Quinta Grande 6, 2780-156 Oeiras, §Centro de Investigação em Ciências da Saúde, Faculdade de Ciências da Saúde, Universidade da Beira Interior, 6201-001 Covilhã, ¶Departamento de Química, Universidade de Évora, P-7000 Évora, ‖Departamento de Química, Faculdade de Ciências e Tecnologia, Universidade Nova de Lisboa, Quinta da Torre, 2829-516 Caparica, Portugal, and **School of Chemistry, University of Southampton, Southampton SO17 1BJ, United Kingdom*

The tetraheme cytochrome c_3 isolated from *Desulfomicrobium baculatum* (DSM 1743) (*Dsmb*) was cloned, and the sequence analysis showed that this cytochrome differs in just three amino acid residues from the cytochrome c_3 isolated from *Desulfomicrobium norvegicum* (*Dsmn*): (*DsmnXXDsmb*) Thr-37 → Ser, Val-45 → Ala, and Phe-88 → Tyr. X-ray crystallography was used to determine the structure of cytochrome c_3 from *Dsmb*, showing that it is very similar to the published structure of cytochrome c_3 from *Dsmn*. A detailed thermodynamic and kinetic characterization of these two tetraheme cytochromes c_3 was performed by using NMR and visible spectroscopy. The results obtained show that the network of cooperativities between the redox and protonic centers is consistent with a synergetic process to stimulate the hydrogen uptake activity of hydrogenase. This is achieved by increasing the affinity of the cytochrome for protons through binding electrons and, reciprocally, by favoring a concerted two-electron transfer assisted by the binding of proton(s). The data were analyzed within the framework of the differences in the primary and tertiary structures of the two proteins, showing that residue 88, close to heme I, is the main cause for the differences in the microscopic thermodynamic parameters obtained for these two cytochromes c_3. This comparison reveals how replacement of a single amino acid can tune the functional properties of energy-transducing proteins, so that they can be optimized to suit the bioenergetic constraints of specific habitats.

A variety of mechanisms used by nature to perform coupled reactions, a fundamental requirement for energy transduction processes, can now be established in detail for relatively small macromolecules that can couple the transfer of electrons and protons.

The tetraheme cytochrome c_3 is found in all organisms belonging to the Desulfovibrionaceae family as well as in other sulfate-reducing bacteria including *Desulfomicrobium* (*Dsm*) species, where it is produced in large quantities (1). It is a soluble protein of low molecular weight, with the *c*-type hemes covalently bound to the polypeptide chain by two thioether bridges provided by cysteine residues arranged in the typical -C*XX*(*XX*)CH-heme binding sequences, and axially coordinated by two histidines.

Recently, tetraheme cytochromes c_3 have been classified as type I and type II (2), and the *Dsm* cytochromes studied in this work have mixed characteristics of both types. Like type I, these cytochromes have a heme-binding site of type -C*XXXX*CH-, acidic residues around heme I, and long N- and C-terminal regions. However, the region of positive charges surrounding heme IV, which is characteristic of type I cytochromes c_3, is not well defined in these cytochromes.

The close proximity of the hemes in cytochrome c_3 results in homotropic redox cooperativities. Furthermore, their reduction potentials are very negative and pH-dependent in the physiological range (redox-Bohr effect) (3, 4). Together, these properties allow cytochromes c_3 to couple the transfer of electrons and protons (5), which for type I cytochrome c_3 (2) is fundamental for its physiological function as partner of the periplasmic hydrogenase (6, 7). The *Desulfomicrobium norvegicum* (*Dsmn*) cytochrome c_3 has been proposed to be involved in electron transfer between the [NiFeSe] hydrogenase and the octaheme cytochrome c_3 (8) in a similar way as that for type I and type II cytochromes c_3 from *Desulfovibrio africanus* (2).

Recent studies allowed the identification of the key residues involved in homotropic and/or heterotropic cooperativities in type I cytochromes c_3 from *Desulfovibrio gigas* (*Dg*) (9) and *Desulfovibrio vulgaris* Hildenborough (*Dv*H) (10, 11). Site-directed mutagenesis studies were used to further probe the role of some specific residues in the modulation of the redox properties of these proteins (12–14). In these cytochromes an anti-electrostatic (conformationally mediated)-positive homotropic cooperativity between two hemes governs a coordinated two-electron transfer, whereas a positive redox-Bohr effect controls their proton thrusting activity. Subsequent characterization of the cytochrome c_3 from *Desulfovibrio desulfuricans* ATCC 27774 (15, 16) illustrated yet another mechanism to facilitate a coordinated two-electron transfer even when there are no positive homotropic redox cooperativities. This alternative mech-

* This work was supported by Fundação para a Ciência e Tecnologia Contracts POCTI/1999/BME/35021, POCTI/2001/QUI/43435, and POCTI/2002/QUI/47866 and Doctoral Fellowships BD/19870/99 (to I. J. C.) and SFRH/BD/6495/2001 (to C. M. P.). The costs of publication of this article were defrayed in part by the payment of page charges. This article must therefore be hereby marked "*advertisement*" in accordance with 18 U.S.C. Section 1734 solely to indicate this fact.

The atomic coordinates and structure factors (code 1w7o) have been deposited in the Protein Data Bank, Research Collaboratory for Structural Bioinformatics, Rutgers University, New Brunswick, NJ (http://www.rcsb.org/).

The nucleotide sequence(s) reported in this paper has been submitted to the GenBank™/EBI Data Bank with accession number(s) AY240938.

‡‡ To whom correspondence should be addressed. Tel.: 351-214469821; Fax: 351-214428766; E-mail: xavier@itqb.unl.pt.

[1] The abbreviations used are: Dsmb, *Desulfomicrobium baculatum* (DSM 1743); Dsmn, *Desulfomicrobium norvegicum*; DvH, *Desulfovibrio vulgaris* (Hildenborough); EXSY, NMR exchange spectroscopy.

TABLE I
Summary of data processing statistics

Nominal resolution range (Å)	21.50–1.81
No. observations	22,339
No. unique reflections	11,633
Completeness (%)	94.4 (80.0)[a]
Multiplicity	1.9 (1.7)[a]
Merging *R* factor (%)	8.0 (18.3)[a]
$\langle I \rangle / \langle \sigma(I) \rangle$	9.1 (3.0)[a]
Wilson B value	31.0 Å^2

[a] Values in parentheses refer to the outer resolution shell 1.88–1.80 Å.

TABLE II
Final refinement statistics summary

Resolution limits (Å)	21.50–1.81
Final free *R* factor (%)	19.1
Final *R* factor (%)	17.6
No. reflections used	
Working set	10,752
Test set	876
No. non-hydrogen protein atoms	1049
No. solvent molecules	72
Model r.m.s. deviations from ideality[a]	
Bond lengths (Å)	0.02
Bond angles (°)	1.84

[a] Root mean square (r.m.s.) = square root of (sum($\mathrm{Geom}_{\mathrm{ideal}} - \mathrm{Geom}_{\mathrm{model}})^2/N_{\mathrm{restraints}}$), where $\mathrm{Geom}_{\mathrm{ideal}}$ is the ideal value for the geometric parameter taken from the dictionary, $\mathrm{Geom}_{\mathrm{model}}$ is the value of the geometric parameter calculated from the current model, and $N_{\mathrm{restraints}}$ is the number of restraints for this particular geometric parameter, over which the summation runs.

anism is achieved by the concerted effect of two positive redox-Bohr effects governing a proton-assisted coordinated two-electron transfer. Furthermore, these positive redox-Bohr effects are also responsible for the proton thrusting activity of this cytochrome (17).

Tetraheme cytochromes c_3 from *Dsm* were isolated from organisms that live in different habitats. *D. norvegicum* (*Dsmn*) (18) was isolated in a pure culture from a saltwater sample from Oslo harbor (19), and *Desulfomicrobium baculatum* (DSM 1743) (*Dsmb*) was isolated from the mud of the Kujalnik estuary near Odessa and Lake Saksky (Crimea) (20) as part of a symbiotic consortium with a green sulfur bacterium (21). However, these two strains have virtually identical 16 S ribosomal RNAs (18), indicating a very close evolutionary proximity. In line with this observation, these *Dsm* cytochromes c_3 have a highly similar primary structure, with Thr-37, Val-45, and Phe-88 in the cytochrome c_3 from *Dsmn* being substituted by Ser, Ala, and Tyr, respectively, in the cytochrome c_3 from *Dsmb*. Also, as shown in this work, its three-dimensional structure, determined by x-ray crystallography, is almost identical to that of Dsmn (22). Nevertheless, as might be expected from the difference in habitat, their microscopic thermodynamic properties are different.

The study of closely similar proteins, such as the natural variants of cytochromes c_3 from *Dsmn* and *Dsmb*, presents the advantage of probing modifications in the primary sequence that are obviously compatible with the maintenance of function. Thus, it may help to characterize the biological factors relevant to the evolution of the protein function.

MATERIALS AND METHODS

Structure Determination of Cytochrome c_3 from Dsmb

Crystallization—The conditions that successfully crystallized cytochrome c_3 from *Dsmn* (23) did not induce any crystals of cytochrome c_3 from *Dsmb*, which was crystallized in 25% PEG_{6K} at a pH between 7.5 and 8.0 using Tris/HCl, 0.1 M as buffer. Thin needles of cytochrome c_3 from *Dsmb* were obtained using the hanging-drop vapor diffusion method. Thicker crystals were obtained when the hanging-drop technique was substituted by the batch technique, which improved the intensity and resolution of the diffraction pattern. Cytochrome c_3 from *Dsmb* crystallizes in the trigonal space group $P3_1$, with cell parameters a = 43.0 Å, b = 43.0 Å, and c = 64.7 Å, with one molecule in the asymmetric unit and a solvent content of 53.3%.

Data Collection—Room temperature diffraction data were collected on a MAR Research detector at station 9.5 at the SRS, CCLRC Daresbury Laboratory, Warrington, UK, using a wavelength of 0.99 Å. The diffraction images were processed and scaled by programs DENZO and SCALEPACK (24); structure factor magnitudes were calculated with the CCP4 package (25). The statistics of the data processing are summarized in Table I.

Structure Determination and Refinement—The structure of cytochrome c_3 from *Dsmb* was solved by molecular replacement using the program AMoRe (26) with the 1.7-Å structure of the cytochrome c_3 from *Dsmn* (22) as a search model. A clear solution with a correlation coefficient of 59.6% and an *R* factor of 34.0% was found.

The first refinement steps, including rigid body minimization, simulated annealing, and a gradual refinement of *B* factors, were performed with X-PLOR (27) using the molecular replacement solution and data to 1.8 Å. The calculated *R* factor at that point was 26.9%. A further stage of refinement was carried out using SHELXL-96 (28) using a restrained conjugated gradient weighted least squares procedure on F^2. During each cycle of refinement a free *R* factor (29) was calculated from 8% of the input 11633 reflections. Following each refinement run, $2m|F_o| - D|F_c|$ and $m|F_o| - D|F_c|$ electron density maps were calculated and inspected on a graphics workstation using TURBO software (30) to adjust incorrect side chain positions to the electron density, to check for previously unseen side chain atoms, and to add water molecules to the model. The criteria followed throughout for including a water molecule were that the corresponding peak should be visible on both the $2m|F_o| - D|F_c|$ and $m|F_o| - D|F_c|$ Fourier maps, and there should be at least one hydrogen bond (between 2.5 and 3.2 Å). The heme irons were refined anisotropically. The main chain positions of loop residues Lys-21 and Gly-22 were not clear, so an omit map was calculated and used for rebuilding the loop. As a result of this procedure the *R* factor was lowered to 16.4% and the final free *R* value to 23.2%. The large difference between the two *R* factors suggested the existence of severe bias in the refined model.

NMR data had shown that Phe-88 was substituted by a Tyr (31), but the sequencing of the cytochrome c_3 gene, which was finished only when the refinement process was started, showed two more differences, Thr-37 and Val-45. Those mutations were introduced in the model and refinement continued with REFMAC version 5.1.24 (32). This program uses maximum likelihood implementation, described as a good tool for improving the diffraction information quality all over the structure. The final refinement statistics are presented in Table II. The refined coordinates and structures factors have been deposited at the Protein Data Bank with the accession code 1w7o.

Cloning and Sequencing of the Dsmb Cytochrome c_3 Gene

Standard protocols were used for DNA manipulation (33). The N-terminal sequence of the first 29 residues of *Dsmb* cytochrome c_3 was found to be identical to the residues of cytochrome c_3 from *Dsmn*. Hence, based on the amino acid sequence available and assuming that the C-terminal sequences of the two cytochromes are also identical, two degenerate oligonucleotides were designed: 5′GAYGCVCCSGGBGAY-GAYTAYG-3′ and 5′RTTSGTSGTRTGRCACTTVCC-3′. By using these primers, *Pfu* polymerase (Stratagene) amplified a 351-bp DNA sequence from the *Dsmb* genomic DNA. The reaction product was cloned into EcoRV cut pZErO™-1 (Invitrogen) vector and transformed into competent cells of *Escherichia coli* XL-2 Blue (Stratagene). Recombinant plasmids were isolated, sequenced on both strands with the ABI Prism BigDye Terminator Cycle Sequencing Ready Reaction kit (PE Biosystems), and analyzed on an Applied Biosystems 377A DNA Sequencer.

Thermodynamic Studies

Sample Preparation—Cytochromes c_3 from *Dsmn* and *Dsmb* were purified as described previously (1), and the NMR samples were prepared at a concentration of 0.5 mM. The ionic strength of the samples was set to ~360 mM through the addition of a concentrated solution of KCl in D_2O to reduce the intermolecular electron transfer rate. The pH of the sample was adjusted for each experiment by adding small volumes of concentrated solutions of DCl and NaOD inside an anaerobic glove box. The pH values reported were not corrected for the isotope effect (34) and cover the range of 4.8–9.6 in *Dsmn* and 4.5–8.8 in *Dsmb*. The reduced and intermediate oxidation states of the protein were obtained by the method described previously (35), using catalytic

amounts of the periplasmic iron hydrogenase isolated from *Dv*H under an H_2 atmosphere as electron donor.

NMR Spectroscopy—Two-dimensional ^{1}H NMR spectra were obtained on a Bruker DRX-500 spectrometer equipped with a 5-mm inverse detection probe with an internal B_0 gradient coil and a BVT3000 temperature controller. The temperature of the samples was kept at 297.0 ± 0.1 K.

The EXSY spectra were acquired with a mixing time of 25 ms and a sweep width of 35 kHz (in both dimensions). The spectra were processed with 1024 × 1024 data points using a Gaussian function in F_2 and sine bell function in F_1. They were calibrated using Tris as internal reference, with the pH-dependent chemical shift of Tris calibrated separately against 2,2-dimethyl-2-silapentanesulfonic acid.

Redox Titrations Followed by Visible Spectroscopy—The redox titrations of both cytochromes were performed at 297.0 ± 1.0 K using an adaptation of the method described previously (15) using ~80 μM protein solutions in 360 mM Tris/maleic acid buffer, pH 6.0, 7.0, and 8.0. The high protein concentration required the use of an optical cell with 1-mm path length to acquire the data. The redox mediators were chosen according to the procedures defined in the literature (36, 37). A mixture of anthraquinone 2-sulfonate (Aldrich), diquat (Riedel den Haan), indigo disulfonate (Merck), indigo trisulfonate (Sigma), methyl viologen (Sigma), neutral red (Sigma), and safranine O (Sigma) was used in all three experiments. In addition to the previous list, gallocyanine (Sigma), 2-hydroxy-1,4-naphthoquinone (Aldrich), indigo tetrasulfonate (Aldrich), and methylene blue (Sigma) were also used at pH 8. At pH 7, anthraquinone 2,7-disulfonate (Aldrich), benzyl viologen (Sigma), 2-hydroxy-1,4-naphthoquinone (Aldrich), indigo tetrasulfonate (Aldrich), and phenosafranine (BDH) were also used, whereas at pH 6 anthraquinone 2,7-disulfonate (Aldrich) and phenosafranine (BDH) were added to the basic mixture of mediators. The final concentration of each mediator was between 4 and 7 μM. To ensure that the results were not subject to interference resulting from specific interactions between the protein and the mediators, several ratios of protein *versus* mediator were tested. A combined Pt/Ag/AgCl electrode was used for measuring the solution potential/ and the reported values are relative to the standard hydrogen electrode.

Kinetic Studies

Sample Preparation—Stock solutions of cytochromes c_3 from *Dsmn* and *Dsmb* were degassed with alternate cycles of argon and vacuum in order to remove the dissolved oxygen and placed in an anaerobic chamber. Dilutions to the desired concentrations were made using 100 mM Tris maleate, pH 5.9, 7.1, and 8.4 for cytochrome c_3 of *Dsmn* and at pH 5.9, 7.2, and 8.4 for cytochrome c_3 of *Dsmb*. The ionic strength was set to ~360 mM through the addition of KCl. After each experiment the actual pH of the reaction was measured, and the concentration of the proteins was determined by UV-visible spectroscopy using ϵ_{552} = 120,000 M^{-1} cm^{-1}.

Sodium dithionite was used as the reducing agent. A large excess of this reagent was used to guarantee pseudo-first order kinetics, irreversible electron transfer steps, and the complete reduction of the cytochrome at every pH value. In order to obtain >95% pure material, the reducing agent was recrystallized inside an anaerobic glove box according to the method described in the literature (38). The solution of sodium dithionite was obtained by adding solid sodium dithionite to degassed 10 mM Tris maleate buffer, pH 8.5, with 360 mM KCl, inside the anaerobic chamber, to give approximately the final desired concentration. The actual concentration of the reducing agent was determined after the experiment, by UV-visible spectroscopy inside the anaerobic chamber, using ϵ_{314} = 8,000 M^{-1} cm^{-1} (39).

Data Collection—The kinetic data were obtained using a stopped-flow instrument (SF-61 HI-TECH Scientific), placed inside an anaerobic chamber. The traces were acquired at 552 nm, and the temperature was maintained at 298.0 ± 1.0 K by the use of an external circulating bath. To perform rapid mixing kinetic experiments starting with various degrees of reduction of the protein sample, a few microliters of concentrated sodium dithionite solution were added to the protein solutions before running the experiments.

Shots of the protein against potassium ferricyanide were made in order to get the reference value for OD^{ox}. To obtain the reference value for OD^{red}, the final absorbance was taken at effectively infinite time after each experiment.

The kinetic curves obtained at different values of solution pH were normalized in order to report oxidized fraction *versus* time. The time scale of the traces was corrected to account for the dead time of the apparatus.

Thermodynamic and Kinetic Modeling—In the redox titrations followed by NMR spectroscopy, the resonance positions and the line widths of one methyl group resonance from each heme were followed in different stages of oxidation, defined by the number of oxidized hemes in the molecule from 0 (fully reduced) to 4 (fully oxidized), and at different pH values. The heme methyl groups $M18^1$ I, $M18^1$ II, $M12^1$ III, and $M18^1$ IV (IUPAC-IUB nomenclature is used to identify the methyl groups and the hemes are indicated by roman numbers according to the order of attachment to the polypeptide chain) were chosen because they point toward the protein surface. Thus, their chemical shifts include only a small extrinsic paramagnetic contribution from the oxidation of the other hemes, which nevertheless was corrected on the basis of calculations using the information from magnetic susceptibility tensors, according to the methods previously described (40–42). After this correction the paramagnetic chemical shift of any heme substituent, in each oxidation stage, is a weighted average of the populations that have this particular heme oxidized in that oxidation stage.

The data obtained by NMR, visible, and stopped-flow kinetics were fitted simultaneously to a thermodynamic model (4, 43) and to a kinetic model (44). The thermodynamic and kinetic models are applicable to systems in fast intramolecular electron transfer and slow intermolecular electron transfer in the time scale of the experiments (3, 44).

Based on the NMR data it is only possible to establish the relative order of oxidation of the hemes, because the solution potential was not measured inside the NMR tube. The calibration of the heme potentials, the heme-heme interactions, and of the redox-Bohr effect was achieved through the redox titrations followed by visible spectroscopy, performed at different pH values.

The kinetic model makes use of the thermodynamic parameters to obtain information on the rate constants for the reduction of the individual hemes. Each heme is characterized by a reference rate constant (k_i^0) that accounts for differences in binding, accessibility to the electron donor, and other structural factors, and it is assumed that this reference constant does not change throughout the reduction process. The actual 64 microscopic rate constants are the product of the reference constant of the heme that is being reduced in a particular microstep and a factor γ_i (Equation 1), derived from Marcus theory (45) that accounts for the thermodynamic driving force (ΔG) of the electron transfer process in that microstep:

$$\gamma_i = \exp\left(\frac{e_i F}{2RT}\left(1 + \frac{e_D F}{\lambda} - \frac{e_i F}{2\lambda}\right)^{-}\right) \qquad \text{(Eq. 1)}$$

Here, e_i is the reduction potential of center i in a particular microstep; e_D is the midpoint potential of the electron donor (SO_2^-), −0.3 V, which is pH-independent (44, 46); and λ is the reorganization energy, assumed to be constant and estimated to be 1 eV (47).

In proteins with intramolecular electron exchange faster than the intermolecular electron transfer from the electron donor, the distribution of electrons inside the multicenter protein is thermodynamically controlled, and it can be considered to equilibrate instantaneously after each one-electron reduction step (44). Therefore, the shape of the kinetic curves contains information about the reduction potentials of the redox centers and their interactions.

The Marquardt method was used to optimize the parameters. The half-height line widths of the NMR signals were used as an estimate of the uncertainty of each chemical shift. The total amplitude of the optical signal in the visible titrations and kinetic experiments were considered to have experimental errors of 3 and 5%, respectively. In addition to the thermodynamic parameters and the four reference rate constants, the chemical shifts for the fully oxidized signals in the deprotonated and protonated forms and the normalization of the visible curves were also optimized (15).

The thermodynamic and kinetic parameters were obtained by the simultaneous fit of thermodynamic and kinetic data. Fitting only the NMR and visible data did not change the thermodynamic parameters significantly (results not shown), showing that the data sets are consistent with the model. However, the simultaneous fit of the NMR, visible, and kinetic data increases the precision of the thermodynamic parameters. Thus, the pH dependence of the kinetic data improved the definition of the pK_a of the acid-base center and the redox-Bohr interactions.

RESULTS

Cloning and Sequencing of the Dsmb Cytochrome c_3 Gene—The complete nucleotide sequence of *Dsmb cytochrome* c_3 was deposited in the EMBL/GenBank™ sequence data base under the accession number AY240938. The amino acid sequence derived from the gene sequence showed that, in fact, the tet-

raheme cytochromes c_3 from *Dsmb* and *Dsmn* are highly homologous, and only three residues (out of 118) were found to be different: (*Dsmn*XX*Dsmb*) Thr-37 → Ser, Val-45 → Ala, and Phe-88 → Tyr.

Analysis of X-ray Structure—The R_{free}/R ratio determined using the final REFMAC refinement values of the structure is 1.08. This value is within the expected range for the number of atoms, refined parameters, and reflections used in a 1.8-Å resolution refinement (48).

The PROCHECK software package (49) was used to analyze the stereochemical quality of the model, and all parameters were found to be within their confidence intervals. In the Ramachandran plot (50) for the refined model of this polypeptide, no residue lies outside the normally allowed regions for non-glycine and non-proline residues, 11.1% lie in the additional allowed regions, and all the others (88.9%) lie in the most favored regions. The ψ, ϕ plots for proline and glycine residues indicate that only Pro-35 presents unusual ψ, ϕ conformation. This residue is positioned between cytochrome c_3 conserved residues Phe-34 and His-36 at the beginning of a small helix region. The electron density map is well defined for that region of the structure. The calculated model G factor, 0.0, is within the normal range for 1.8-Å resolution structures. The dispersion precision indicator was estimated as 0.143 Å (51).

A good connectivity was found for the whole structure, except for the 20–26 external loop. In the final Fourier maps, it was not possible to locate the side chain atoms of some residues; therefore, these atoms were included in the model with zero occupancy. Almost all residues in this situation have long side chains and are located at the protein surface.

The highest main chain *B* factors correspond to mobile loop regions, and the highest side chain *B* factors correspond to long side chain residues located on the protein surface. The average *B* factor for all protein atoms is 28.1 Å^2; the solvent molecules have an average *B* factor of 35.4 Å^2, and the heme groups have an average of 21.4 Å^2. The amino acid sequence differences between cytochrome c_3 from *Dsmn* and from *Dsmb* became evident during the refinement.

Comparison with the Structure of Cytochrome c_3 from Dsmn—Cytochromes c_3 from *Dsmb* and from *Dsmn*, which have only three amino acid residues different, present very similar structures. The root mean square of the main chain, and all atom coordinate deviations, calculated after superposing both main chain structures are 0.265 and 0.605 Å, respectively. The largest main chain deviation occurs for loop 20–26, an external loop in a solvent channel without any packing interactions. Other main chain deviations and side chain deviations occur mainly for surface residues.

The intramolecular iron-iron distances and the interplanar angles for the heme porphyrin rings, the hydrogen-bonding schemes of the heme-coordinating histidine residues, and the angle between the planes of their imidazole rings of cytochrome c_3 from *Dsmb* are very similar to those observed for cytochrome c_3 from *Dsmn*.

The relative solvent accessibility to the heme groups was calculated using X-PLOR and the Lee and Richards algorithm (52) with an H_2O probe radius of 1.6 Å. First, the solvent-accessible surface was calculated for each residue in the structure; next the same calculation was performed for the same residue, in the same conformation as in the molecule but isolated from the rest of the structure. The ratio of these two values for each residue is its relative solvent accessibility. Comparing these results with those obtained for cytochrome c_3 from *Dsmn* in a similar calculation, it can be seen that all values are very similar, as expected. The larger difference is for heme II, where propionate 13 has a completely different conformation from that found in cytochrome c_3 from *Dsmn*. In cytochrome c_3 from *Dsmb*, O1D is H-bonded to a water molecule that interacts with His-49 N-δ1 and Lys-97 N-ζ. This conformation of propionate 13 induces a different conformation in the side chain of Ile-81; no interactions are observed for O1D of propionate 13 of heme II from *Dsmn* cytochrome c_3.

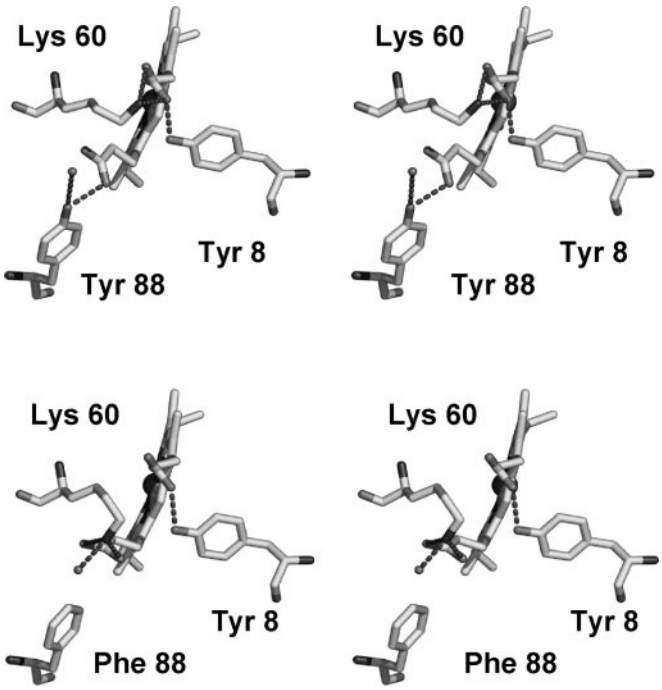

FIG. 1. **Propionate interactions of heme I in cytochrome c_3 from *Dsmb* and *Dsmn* structures.** The distance between Tyr-8 OH and O2A is 2.61 Å for both structures. The additional interaction observed in cytochrome c_3 from *Dsmb* structure is established between Tyr-88 OH and O2D (distance 2.56 Å). Drawings were made with Pymol software (DeLano Scientific, San Carlos, CA).

In cytochrome c_3 from *Dsmb* Ser-37 C-β and O-γ positions superimpose with cytochrome c_3 from *Dsmn* Thr-37 C-β and O-γ1 positions, and in cytochrome c_3 from *Dsmb* Ala-45 substitutes another non-polar residue, Val-45, localized at the protein surface in a solvent channel. In both cases, no significant structural differences were noticed. However, the replacement of Phe-88 by a polar residue in cytochrome c_3 from *Dsmb* allows the establishment of two additional H-bonds, between Tyr-88 OH, a water molecule, and an oxygen atom of propionate 13 of heme I. Lys-60 side chain adopts a different conformation, and the N-ζ is H-bonded to propionate 17 oxygen atoms in *Dsmb*, instead of propionate 13. Although the crystallization conditions of the two proteins are different, they are not expected to lead to the observed differences in the hydrogen bonding network because the pH values were similar and above the functional pK_a values (see below). Fig. 1 shows the H-bonding network involving the propionates of heme I, Tyr-8, Tyr-88, and Lys-60.

Thermodynamic and Kinetic Properties—The proteins studied in this work, cytochromes c_3 from *Dsmn* and *Dsmb* (both with pI ≈7), present a small formal charge in a wide range of pH values around neutrality, which facilitates a close contact among different molecules in solution and increases the intermolecular electron exchange rate (31). As a consequence, previous redox titrations followed by NMR spectroscopy of these two proteins were performed in conditions of intermediate to fast intermolecular electronic exchange on the NMR time scale (31, 53), which only allowed the determination of macroscopic thermodynamic parameters. A different set of macroscopic thermodynamic parameters was obtained through EPR studies

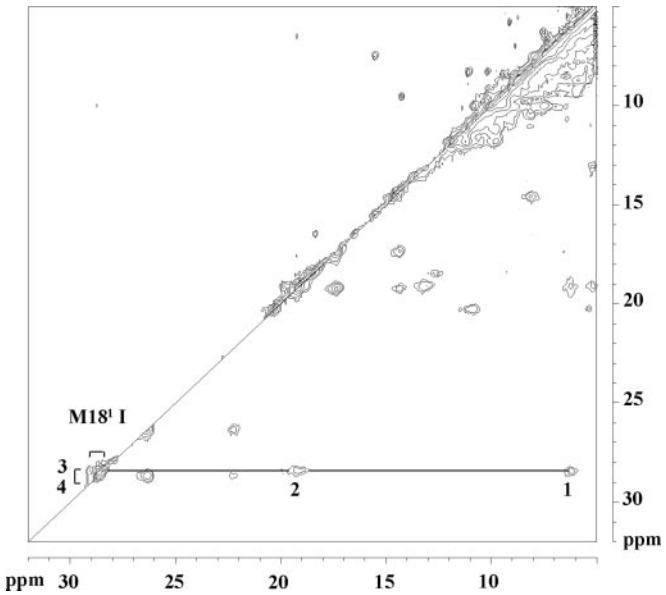

FIG. 2. **EXSY spectra of cytochrome c_3 of *Dsmn* in different stages of oxidation.** Each stage contains all microstates with the same number of oxidized hemes, zero for fully reduced to four to fully oxidized. In the spectrum *below the diagonal* (pH 7.2), oxidation stages 1–3 are shown. Stages 3 and 4 are presented *above the diagonal* (pH 7.3). These show the pattern characteristic for slow inter- and fast intramolecular electronic exchange. The lines connect signals from M18[1] I at different redox stages, indicated in the figure by the *numbers 1–4.* Signals of the protein in the fully reduced stage are not visible in these experiments.

(54, 55). In the present study, the intermolecular electronic exchange rate was slowed by increasing the ionic strength, lowering the temperature, and lowering the sample concentration (56). In conditions of slow intermolecular electron exchange but fast intramolecular electron exchange, each heme substituent displays five discrete NMR signals corresponding to each of the five redox stages connected by four steps of a single electron transfer (3). Because most heme methyl group resonances are shifted by the paramagnetic effect to less crowded regions of the NMR spectra, they are usually easy to follow (Fig. 2). The simultaneous fits of the thermodynamic and kinetic models to the data of the redox titrations obtained by NMR, visible spectroscopy, and kinetic traces are shown in Figs. 3–5.

In the redox titrations followed by NMR, there is good agreement between the experimental data and the fit for both proteins. The deviation between the fitted line and the experimental points of cytochrome c_3 *Dsmn* M18[1] I in stage 2, in the region of pH 5.7, reflects the larger uncertainty in the measurement. This uncertainty is caused by the broadening of the NMR signals at pH values close to the pK_a, as reported for other cytochromes (4, 17). The small pH dependence of the chemical shifts of the heme substituents in the fully oxidized protein shows that the acid-base center has little effect on the electronic structure of the hemes (4, 42). The largest variations in chemical shift are observed for the intermediate stages of oxidation and result from changes in the relative reduction potentials of the hemes with pH (3, 4, 57).

The fit obtained for the redox titrations followed by visible spectroscopy is also good (Fig. 4). The titrations of cytochrome c_3 from *Dsmb* show smaller pH dependence in the pH range covered by this study than those of cytochrome c_3 from *Dsmn*, in agreement with the NMR and kinetic data.

Tables III and IV report the microscopic thermodynamic parameters obtained by fitting the model of five interacting centers to the experimental data. The diagonal elements are the free energies necessary to oxidize the four hemes and to deprotonate the acid-base center, in the protonated form of the protein. Above the diagonal are the interaction energies between each pair of hemes (homotropic cooperativities) and the interaction energies between the redox centers and the acid-base center (heterotropic cooperativities). The large separation between the reduction potential of heme III and the reduction potentials of the other hemes, as well as the lack of observable NMR signals from heme III in stages 1 and 2, precludes the determination of heme-heme interactions involving this heme. Therefore, only 12 parameters were determined in the present study (Tables III and IV). The free energies for oxidizing hemes I, II, and IV are defined for the fully reduced state of the protein. However, because heme III is the last heme to be oxidized, and is well separated from the others, its free energy of oxidation can only be evaluated for the situation in which hemes I, II, and IV are already oxidized. This means that all heme-heme interactions involving heme III are included in the free energy of oxidation reported for it in Tables III and IV. The energies of oxidation of the hemes, expressed in meV, have the same numerical value as the reduction potentials expressed in mV.

The pK_a value of the acid-base center depends on the degree of oxidation of the cytochrome because of the redox-Bohr interactions. The values for each stage are reported in Table V.

The present results confirm the order of oxidation of the hemes of cytochrome c_3 from *Dsmb* at pH 7.8 and of cytochrome c_3 from *Dsmn* at pH 9.0, as reported for these proteins (53), heme II, heme I, heme IV, and then heme III. Most interestingly, although there is no change in the order of oxidation for cytochrome c_3 from *Dsmb* in the pH range studied, the order of oxidation of hemes I and IV is reversed at lower pH values in cytochrome c_3 from *Dsmn* (Fig. 6). This difference is caused by small synergetic changes in the thermodynamic parameters of the two cytochromes.

The kinetic data obtained for the reduction of the two cytochromes c_3 with sodium dithionite at different pH values are presented in Fig. 5. The figure also shows the fitted curves obtained with the kinetic model, using the thermodynamic parameters listed in Tables III and IV and the rate constants reported in Tables VI and VII, which show an excellent agreement with the experimental data. The rate constants obtained from single exponential fitting of the kinetic traces show a linear dependence on the square root of the concentration of sodium dithionite, indicating that the reducing agent for both *Dsmb* and *Dsmn* cytochromes c_3 is SO_2^- (data not shown and see Ref. 58). The reference rate constants, k_i^0, for both cytochromes are shown in Tables VI and VII. In both cytochromes, the rate constant for heme II is the largest. In order to compare the relative importance of the hemes in the reduction process, the fraction of electrons that enters the molecule through each heme in each reduction step at each pH was calculated for both cytochromes (Tables VIII and IX). The kinetic behavior of the two cytochromes is very similar. In the first reduction step the electrons enter the molecule through hemes II and III. Although the reference rate constant of heme III is ~20 times smaller than that of heme II, the much larger driving force for the reduction of heme III in step 1 compensates for this difference, and in this step heme III receives electrons from SO_2^- at a slightly higher rate than heme II. In the remaining reduction steps most electrons enter the molecule through heme II. However, heme II drains electrons to hemes I and IV via intramolecular electron transfer and is the last heme to become fully reduced. There is some contribution from heme I in reduction steps 1–3, which is more important in cytochrome c_3 from *Dsmb*. However, this difference lacks sta-

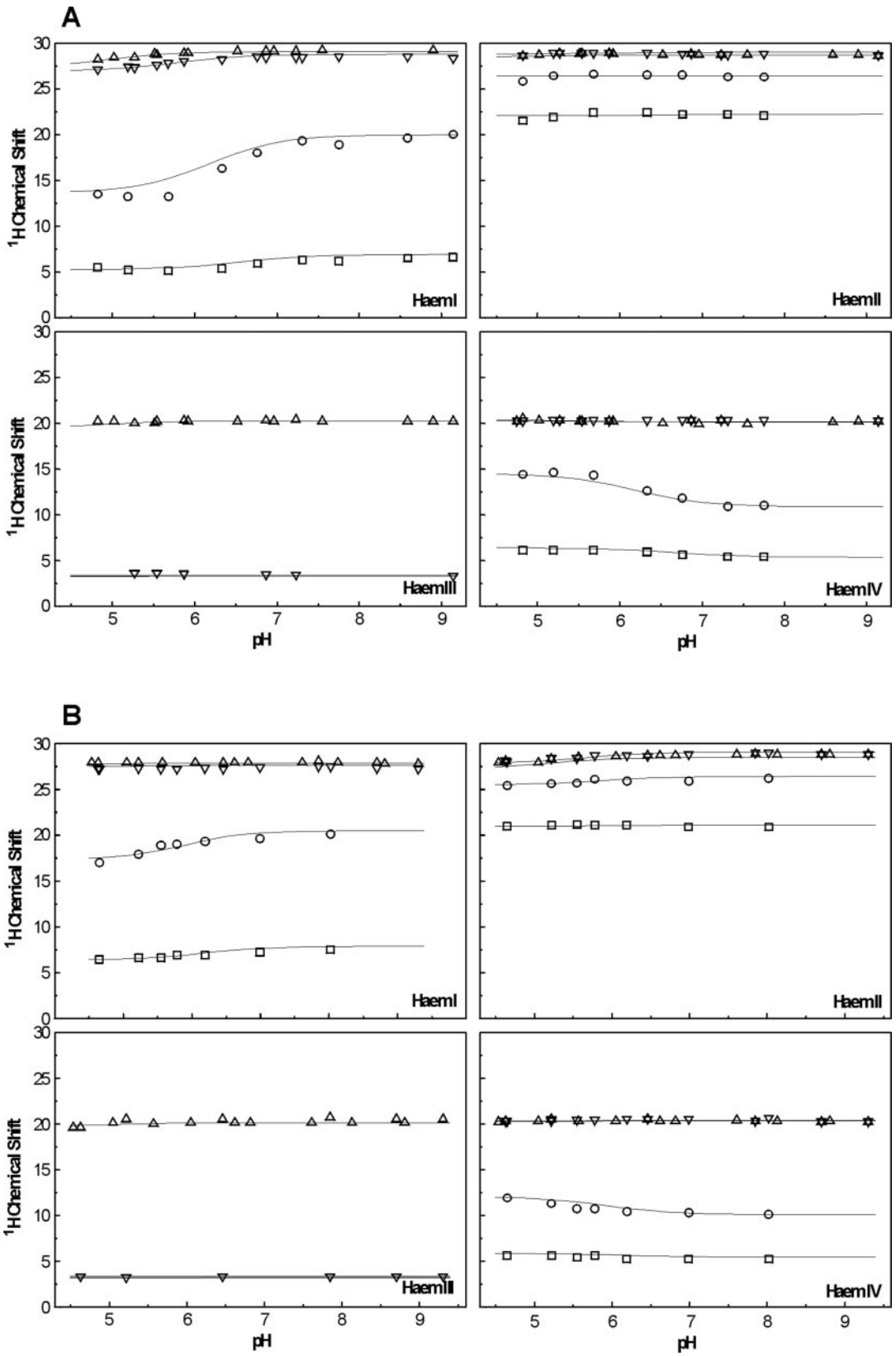

FIG. 3. **pH dependence of the ^{1}H chemical shifts of one methyl group from each of the four hemes of cytochrome c_3 from *Dsmn* (*A*) and from *Dsmb* (*B*), in different stages of oxidation at 297 ± 0.1 K.** Stages of oxidation 1–4 are represented by the symbols as follows: stage 1, □; stage 2, ○; stage 3, ▽; and stage 4, △. The *full lines* represent the best fit of the data to the model of the five charged centers (Tables III and IV). The chemical shifts for stage 1 and 2 of M12^1 III were not determined because they could not be identified unequivocally in the crowded diamagnetic region of the spectra.

tistical significance because the standard errors associated with the reference rate constants of heme I are very large.

The central assumption of the kinetic model, that the changes in the rate constants for electron transfer are determined by variations in the driving force, is tested most clearly in relation to the pH dependence of the rates. The fact that

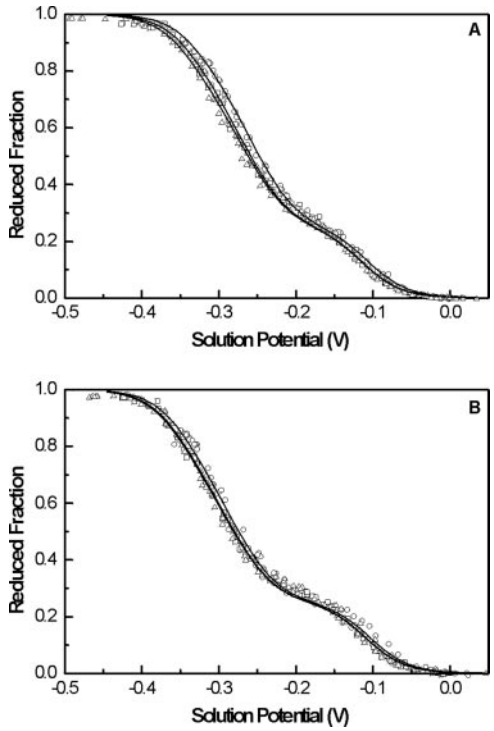

FIG. 4. **Relative OD of the total reduced cytochrome c_3 from *Dsmn* (*A*) and *Dsmb* (*B*) determined by visible spectroscopy at pH 6 (○), 7 (□), and 8 (Δ).** The *lines* represent the best fit of the experimental data to the five center model (Tables III and IV).

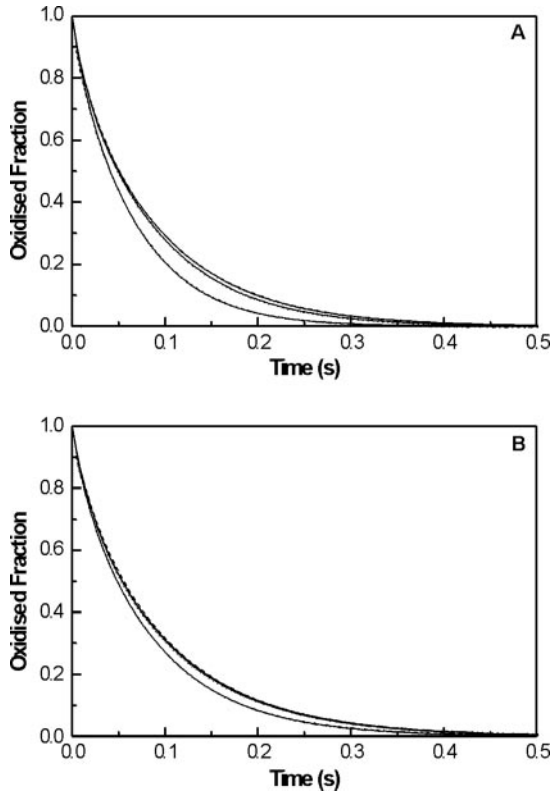

FIG. 5. **Kinetics of reduction of cytochrome c_3 from *Dsmn* and *Dsmb* by sodium dithionite at different pH values.** Rates increase with decreasing pH. *A, Dsmn* cytochrome at pH 8.4 (*dash*), pH 7.1 (*dot*), and pH 5.9 (*dash-dot*). The concentration of dithionite was 140 μM and the concentration of protein was 0.9, 0.9, and 0.7 μM for the different pH values, respectively. *B, Dsmb* cytochrome at pH 8.4 (*dash*), pH 7.2 (*dot*), and pH 5.9 (*dash-dot*). The concentration of dithionite was 185 μM, and the concentration of protein was 0.8, 0.9, and 0.7 μM for the different pH values, respectively. *Continuous lines* are the fit to the data.

simultaneous fitting of thermodynamic and kinetic data did not change the values of the thermodynamic parameters obtained from fitting the thermodynamic data alone shows that the data are consistent with the model.

The relative accessibility of the hemes to the reducing agent, which can be determined from the crystal structure, is one of the factors that may influence the reference rate constants. This was calculated on the basis of the surface accessibility of the heavy atoms of the porphyrin to a sphere of radius of 2.5 Å, assuming that the contribution of the α-substituents have 10 times less weight than those of the macrocycle. The values obtained for the two cytochromes are presented in Tables X and XI.

The exposure of the hemes to the reducing agent appears to be the most important factor in determining which heme acts as the main gate for entrance of electrons in these proteins, when using dithionite as the reducing agent. In both cytochromes, heme II is the most exposed (Tables X and XI) and is the heme with the larger reference rate constant. Nevertheless, the absence of a direct relationship between the relative accessibilities and the values of the reference rate constants of the different hemes shows that accessibility is not the only structural factor controlling the rates, as would be expected because the reducing agent is a small charged molecule.

Because the experimental conditions of the kinetic experiments were the same and the two proteins studied are almost identical structurally, the reference rate constants of the two proteins should be very similar, and this is confirmed by the results (Tables VI and VII).

DISCUSSION

Structural Interpretation of the Thermodynamic Properties—The redox parameters presented in Tables III and IV show that heme II has the lowest reduction potential in both proteins, which correlates with the largest solvent exposure (22). Hemes I and IV of both cytochromes c_3 have similar reduction potentials. Heme III, which is partly shielded from the solvent by the polypeptide chain, has the highest midpoint reduction potential, well separated from those of the other three hemes.

The polypeptide chains of the two proteins differ only by three amino acid residues, in positions 37, 45, and 88. In both cases, the side chains of the amino acid residues in positions 37 and 45 are pointing toward the surface of the protein and are relatively far from the hemes and the acid-base center involved in the redox-Bohr effect (see Ref. 22 and present work). Consequently, these residues should have a negligible effect in controlling the redox and acid-base properties of any of the centers. In contrast, the only non-neutral mutation, residue 88 that is a Phe in the cytochrome from *Dsmn* and a Tyr in the cytochrome from *Dsmb*, is buried in the interior of the protein close to heme I. The reduction potentials of the hemes in cytochrome c_3 from *Dsmb* are more negative than those of *Dsmn*, with heme I displaying the larger difference, 37 mV, compared with differences around 20 mV for the other three hemes (Tables III and IV). The more negative reduction potentials in *Dsmb* may be a consequence of the stabilization of the charged form of the hemes (the oxidized one) in the more polar environment of the Tyr 88 hydroxyl group, which makes the reduction of this cytochrome more difficult. The location of Tyr-88 close to heme I is compatible with the larger difference observed for the reduction potential of this heme.

The heme-heme interactions are all anticooperative (positive free energies). Their values are very similar in the two cytochromes, as expected, given the high degree of structural similarity between the two proteins.

The redox and acid-base centers display positive cooperativities (negative free energies). All interactions are well defined,

TABLE III

Thermodynamic parameters determined by fitting the 5-center model to the NMR, visible and kinetic data from Dsmn cytochrome c_3

The fully reduced and protonated protein was taken as the reference state for all hemes except heme III. The reference for heme III is the protonated protein in stage 3. The diagonal terms, in boldface, are the energies for oxidation of the hemes and for the deprotonation of the ionizable centers, whereas the off-diagonal terms are the redox and redox-Bohr interaction energies. All values are reported in meV. Values within parentheses are the S.E. The pK_a value of the acid-base center can also be calculated from the ΔG (in meV) using the relationship p$K_a \approx \Delta G/60$.

Dsmn c_3	Energies				
	Heme I	Heme II	Heme III	Heme IV	Ionizable center
			meV		
Heme I	**−257** (2)	15 (2)		12 (2)	−37 (3)
Heme II		**−312** (2)		20 (2)	−24 (2)
Heme III			**−62** (2)		−53 (8)
Heme IV				**−274** (2)	−13 (3)
Ionizable center					**413** (4)

TABLE IV

Thermodynamic parameters determined by fitting the 5-center model to the NMR, visible, and kinetic data from Dsmb cytochrome c_3

The fully reduced and protonated protein was taken as the reference state for all hemes except heme III. The reference for heme III is the protonated protein in stage 3. The diagonal terms, in boldface, are the energies for oxidation of the hemes and for the deprotonation of the ionizable centers, whereas the off-diagonal terms are the redox and redox-Bohr interaction energies. All values are reported in meV. Values within parentheses are the S.E. The pK_a value of the acid-base center can also be calculated from the ΔG (in meV) using the relationship p$K_a \approx \Delta G/60$.

Dsmb c_3	Energies				
	Heme I	Heme II	Heme III	Heme IV	Ionizable center
			meV		
Heme I	**−293** (2)	13 (2)		14 (2)	−23 (3)
Heme II		**−336** (2)		18 (2)	−13 (2)
Heme III			**−79** (2)		−31 (10)
Heme IV				**−294** (3)	−9 (3)
Ionizable center					**378** (5)

TABLE V

Macroscopic pK_as for the ionizable center associated with each of the five stages of oxidation for cytochromes c_3 of Dsmn and Dsmb

	Ionizable center				
	Stage 0	Stage 1	Stage 2	Stage 3	Stage 4
Dsmn	7.0	6.6	6.2	5.7	4.8
Dsmb	6.4	6.2	5.9	5.6	5.1

with the exception of the redox-Bohr interactions with heme III in both cytochromes. The uncertainty in this value is linked to a poor definition of the pK_a of the oxidized form, due to lack of experimental data at low pH values. Therefore, there is little purpose in any comparison involving the value of the pK_a^{ox} or the heme-proton interaction with heme III, but this does not affect the main points of discussion because, as mentioned above, heme III essentially titrates on its own. In this context, heme I has the strongest of all the significant interactions with the protonic center in both proteins. This makes propionate 13 of heme I a likely candidate for the redox-Bohr group, as proposed previously for other cytochromes c_3 (4, 13, 17, 40, 59). In *Dsmb* the hydroxyl group of Tyr-88 is pointing to propionate 13 of heme I and is at a distance of 2.56 Å. This distance is compatible with the formation of hydrogen bonds (Fig. 1). The extra hydrogen bond between Tyr-88 and propionate 13 of heme I of cytochrome c_3 from *Dsmb* contributes to an extra stabilization of the deprotonated form of this propionate. Indeed, the acid-base center of cytochrome c_3 from *Dsmb* has a lower pK_a value in the reduced state (Table V), which corresponds to the uncharged form of the heme. The difference in macroscopic pK_a values between the two cytochromes fades as oxidation progresses, possibly due to a difference in shielding of the electrostatic interaction between the positive charge of the heme and the negative charge of the propionate (60). The stabilization of the propionate, when going from the reduced to the oxidized form (causing a pK_a drop), should be smaller in the cytochrome from *Dsmb*, due to the presence of the more polar Tyr-88, and this is indeed the case (Table V). This effect is also reflected by the smaller redox-Bohr interactions found in *Dsmb* cytochrome c_3 when compared with those of *Dsmn*. The difference in the redox-Bohr interactions determined for the two proteins is easily detected in the pH dependence of their visible titrations (Fig. 4) and the kinetic curves (Fig. 5).

Mechanistic Interpretation of the Functional Thermodynamic Properties—The hypothesis is that the physiological function of type I cytochrome c_3 is to accept electrons and protons from the periplasmic hydrogenase and deliver them to membrane-linked proteins, including the type II cytochrome c_3, with a net energy transfer from the redox to the protonic centers (5, 7, 17). There are several requirements for a soluble protein to act as an efficient electron-proton energy transducer, not all of which can be established by studying the protein in isolation (61, 62). The first requirement is that the centers are thermodynamically coupled, which is clearly demonstrated by the results presented here. Second, the coupling should be effective under physiological conditions, which is apparent when the redox state-dependent pK_a values span the physiological pH range. With reference to Fig. 7, and by analogy with other cytochromes c_3 that have been characterized (4, 63), the best candidates for electron-proton energy transduction in the *Dsm* cytochromes are states of the redox stages 1 and 3; a deprotonated state of the cytochrome in stage 3 is ready to receive electrons and protons from hydrogenase, giving a protonated state of stage 1 (Fig. 7). Fig. 7*A* shows the populations of the various microstates as a function of solution potential at pH 6.15. Stages 1 and 3 both have significant populations at intermediate potentials. The lowest energy microstates at pH 6.15 and a solution potential −260 mV are shown in Fig. 7*B*. Clearly, a transfer of two electrons coupled to protonation is thermodynamically favorable, whereas the transfer of a second electron without protonation would be thermodynamically less favorable. In fact, docking studies suggest that electrons will be transferred from hydrogenase to cytochrome c_3 via heme IV (64). This fits very well with the energies of the microstates shown in Fig 7*B*. The most stable form in stage 3 is deprotonated and has hemes I, II, and IV oxidized; reducing heme IV

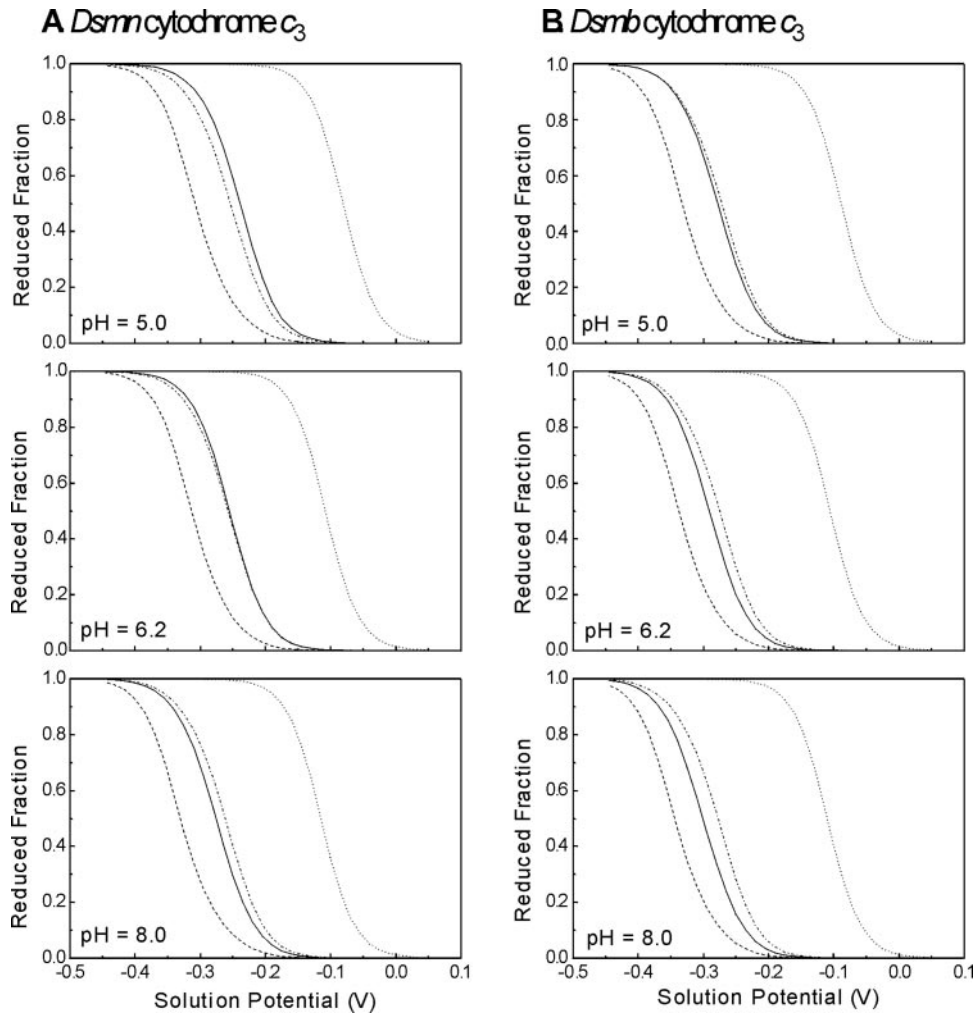

FIG. 6. **Reduction profiles of individual hemes from *Dsmn* cytochrome c_3 (*A*) and *Dsmb* cytochrome c_3 (*B*), at different pH values, calculated from the thermodynamic parameters.** Hemes I, II, III, and IV are represented by *continuous, dashed, dotted*, and *dash-dot lines*, respectively. In cytochrome c_3 from *Dsmn,* hemes I and IV change their order of oxidation in this pH range.

TABLE VI
Reference rate constants for each heme, k_i^o, for Dsmn cytochrome c_3
Standard errors with respect to an experimental error of 5% in the kinetic traces are given in parentheses.

Dsmn	Heme I	Heme II	Heme III	Heme IV
Reference rate constants k_i^0 ($\times 10^8$ M^{-1} s^{-1})	5 (11)	97 (7)	5.1 (0.8)	1 (10)

TABLE VII
Reference rate constants for each heme, k_i^o, for Dsmb cytochrome c_3
Standard errors with respect to an experimental error of 5% in the kinetic traces are given in parentheses.

Dsmb	Heme I	Heme II	Heme III	Heme IV
Reference rate constants k_i^0 ($\times 10^8$ M^{-1} s^{-1})	16 (9)	98 (10)	3.4 (0.6)	0 (6)

allows rapid conversion through protonation and intramolecular electron transfer to a microstate that has hemes II and IV oxidized. Transferring a second electron to heme IV yields the most stable microstate of stage 1, a protonated form with only heme II oxidized. Thus, the redox-Bohr effects on hemes I and IV result in a reduction of the electrostatic penalty associated with the coordinated transfer of two electrons, which in cytochrome c_3 from *Dsmn* even leads to a permutation of the order of oxidation of these two hemes in the physiological pH range.

As both reductions have positive redox-Bohr effects, *cf.* Tables III and IV, it is ensured that the affinity for protons of the cytochrome increases, which is critical for stimulating the activity of hydrogenase at low pH values (7). However, and most importantly, the involvement of the positive redox-Bohr cooperativities is not confined to the activation of protons. In fact, the obligatory reciprocity of interactions results in promoting a coordinated transfer of two electrons. Subsequently, the electrons are released to a transmembrane electron transfer complex, and the protonic center of the reoxidized cytochrome is acidified, releasing protons that can be thrusted to activate ATP synthase (17, 61, 62), thus avoiding uncoupled transfer of electrons and protons that would lead to short-circuiting the energy-transducing process. However, this order of events, although probable on the basis of typical electron and proton transfer rates, cannot be deduced from the thermodynamic properties of the isolated cytochrome. Nevertheless, the reduction potentials of the isolated cytochrome are sufficiently close

TABLE VIII
Fraction of electrons that enter the molecule through each heme in each one-electron reduction step, calculated using the thermodynamic parameters of Tables III and IV and the reference rate constants of Table VI and VII

For *Dsmn*, cytochrome *c*, the values were calculated for pH 5.9, 7.1, and 8.4.

pH	Step	Heme I	Heme II	Heme III	Heme IV
5.9	1	0.04	0.38	0.57	0.01
	2	0.10	0.87	0.01	0.02
	3	0.07	0.92	0.00	0.01
	4	0.02	0.98	0.00	0.00
7.1	1	0.04	0.39	0.56	0.01
	2	0.09	0.88	0.01	0.02
	3	0.07	0.91	0.00	0.01
	4	0.02	0.98	0.00	0.00
8.4	1	0.04	0.39	0.56	0.01
	2	0.09	0.88	0.01	0.02
	3	0.08	0.91	0.00	0.01
	4	0.02	0.97	0.00	0.00

TABLE IX
Fraction of electrons that enter the molecule through each heme in each one-electron reduction step, calculated using the thermodynamic parameters of Tables III and IV and the reference rate constants of Table VI and VII

For *Dsmb*, cytochrome c_3 the values were calculated for pH 5.9, 7.2, and 8.4.

pH	Step	Heme I	Heme II	Heme III	Heme IV
5.9	1	0.11	0.36	0.53	0.00
	2	0.24	0.76	0.00	0.00
	3	0.19	0.81	0.00	0.00
	4	0.07	0.93	0.00	0.00
7.2	1	0.11	0.37	0.52	0.00
	2	0.22	0.77	0.00	0.00
	3	0.19	0.81	0.00	0.00
	4	0.08	0.92	0.00	0.00
8.4	1	0.11	0.37	0.52	0.00
	2	0.22	0.78	0.00	0.00
	3	0.19	0.81	0.00	0.00
	4	0.08	0.92	0.00	0.00

TABLE X
Relative accessibility of SO_2^- to the hemes of cytochrome c_3 from Dsmn

The values were calculated for a sphere of radius 2.5 Å.

Dsmn	Heme I	Heme II	Heme III	Heme IV
Relative accessibility	2.60	7.62	1.58	4.49

TABLE XI
Relative accessibility of SO_2^- to the hemes of cytochrome c_3 from Dsmb

The values were calculated for a sphere of radius 2.5 Å.

Dsmb	Heme I	Heme II	Heme III	Heme IV
Relative accessibility	2.22	5.88	2.00	4.72

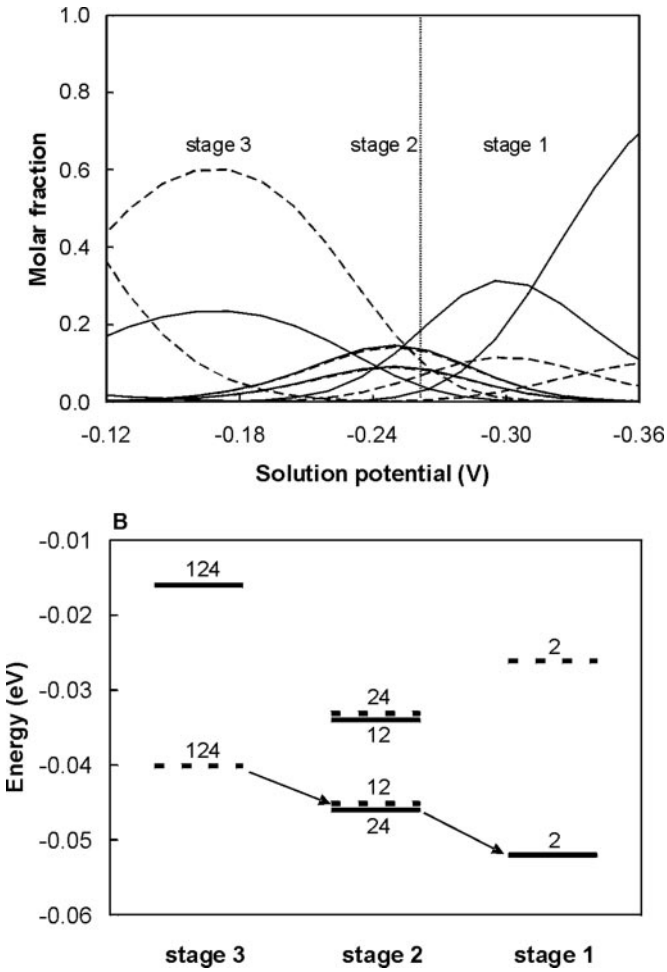

FIG. 7. *A*, populations of microstates at pH 6.15 plotted as a function of solution potential. The populations were calculated from the values of the thermodynamic parameters in Tables III and IV using the equations reported in Turner *et al.* (4). Note that stage 2 (two hemes oxidized) is never highly populated. The situation for the most highly populated (lowest energy) microstates at an intermediate solution potential (indicated by a *dashed line*) is shown in more detail in *B*. *B*, energy level diagram of microstates in stages 1–3. Energies (relative to the fully reduced and protonated protein) were calculated from the values of the thermodynamic parameters in Tables III and IV using the equations reported in the literature (4). The conditions chosen, a solution potential of −260 mV and pH 6.15, should approximate those in the periplasm. Only the 8 microstates with lower energies are shown, out of a total of 32 for the 5 oxidation stages. Protonated microstates are represented with *solid lines* and deprotonated forms with *dashed lines*. The relevant microstates in stage 3 have hemes I, II, and IV oxidized; those in stage 2 have either hemes I and II or II and IV oxidized, and only heme II is oxidized in stage 1. If a cytochrome molecule in stage 3 receives two electrons, the most stable (lowest energy) form clearly switches from being deprotonated to protonated; the path for consecutive electron transfers to heme IV is indicated by *arrows* (see text). For clarity, *arabic numbers* were used for the hemes in the figure.

to make a coordinated two-electron transfer possible, such that a slight change in conformation caused by the protein-protein interaction can easily shift the balance to make it effective. It is reasonable to assume that this small but complex molecule has evolved to a high degree of efficiency to carry both the protons and the electrons generated from the oxidation of hydrogen. Although at present there is no experimental evidence for a second proton-binding site, an extra proton could be accommodated through small changes in the populations at a number of other sites and assist the two-electron transfer as seen in cytochrome c_3 from *D. desulfuricans* 27774 (15, 16).

It is likely that the changes in thermodynamic parameters that occur when the transducer donor-acceptor complex is formed will improve the functional properties. Thus, novel methodologies must be developed to characterize the functional multicomponent systems to discover how this potential is realized in the physiological context.

Conclusions—The thermodynamic parameters obtained for these two *Dsm* cytochromes suggest that they are capable of performing e^-/H^+ energy transduction using a different mechanism from that described previously (4, 17, 40, 43, 65) for *D. vulgaris* and *D. gigas* type I cytochromes c_3. The variations in the microscopic thermodynamic parameters of these two phylogenetically related strains are caused by a small difference in their amino acid sequences and may have resulted from evolutionary advantages associated with the different habitats from which these two organisms were isolated. *Dsmn* was obtained as a pure culture, and consequently this strain is more

dependent on the environmental conditions of the habitat. On the other hand, *Dsmb* was isolated from a symbiotic association between green sulfur bacteria and sulfate-reducing bacteria (21). Curiously, the primary electron acceptor of the anoxic phototrophic process is poised at a very low redox potential. The maintenance of a closed sulfur cycle by the symbiotic association involving *Dsmb* may require a different tuning of the thermodynamic properties of proteins involved in the bioenergetic processes.

Acknowledgments—We thank Prof. A. Netrusov for providing the references to identify the place from which the symbiont *Chloropseudomonas ethylica* was isolated. We thank the fermentation plant at the University of Georgia, Athens, for growing the bacteria, and we also thank Isabel Pacheco and Dr. Isabel Coutinho (Instituto de Tecnologia Química e Biológica, Universidade Nova de Lisboa) for the purified samples used for crystallization. Crystallographic studies were funded by European Union Grant HCM-CHRX-CT93–0143 and were supported by the Council for the Central Laboratory of the Research Councils in the Daresbury Laboratory (Warrington, UK).

REFERENCES

1. Coutinho, I. B., and Xavier, A. V. (1994) *Methods Enzymol.* **243,** 119–140
2. Valente, F. M., Saraiva, L. M., LeGall, J., Xavier, A. V., Teixeira, M., and Pereira, I. A. (2001) *Chembiochem.* **2,** 895–905
3. Santos, H., Moura, J. J., Moura, I., LeGall, J., and Xavier, A. V. (1984) *Eur. J. Biochem.* **141,** 283–296
4. Turner, D. L., Salgueiro, C. A., Catarino, T., LeGall, J., and Xavier, A. V. (1996) *Eur. J. Biochem.* **241,** 723–731
5. Xavier, A. V. (1986) *J. Inorg. Biochem.* **28,** 239–243
6. Yagi, T., Honya, M., and Tamiya, N. (1968) *Biochim. Biophys. Acta* **153,** 699–705
7. Louro, R. O., Catarino, T., LeGall, J., and Xavier, A. V. (1997) *J. Biol. Inorg. Chem.* **2,** 488–491
8. Aubert, C., Brugna, M., Dolla, A., Bruschi, M., and Giudici-Orticoni, M. T. (2000) *Biochim. Biophys. Acta* **1476,** 85–92
9. Brennan, L., Turner, D. L., Messias, A. C., Teodoro, M. L., LeGall, J., Santos, H., and Xavier, A. V. (2000) *J. Mol. Biol.* **298,** 61–82
10. Matias, P. M., Frazao, C., Morais, J., Coll, M., and Carrondo, M. A. (1993) *J. Mol. Biol.* **234,** 680–699
11. Messias, A. C., Kastrau, D. H., Costa, H. S., LeGall, J., Turner, D. L., Santos, H., and Xavier, A. V. (1998) *J. Mol. Biol.* **281,** 719–739
12. Saraiva, L. M., Salgueiro, C. A., LeGall, J., van Dongen, W. M. A. M., and Xavier, A. V. (1996) *J. Biol. Inorg. Chem.* **1,** 542–550
13. Saraiva, L. M., Salgueiro, C. A., da Costa, P. N., Messias, A. C., LeGall, J., van Dongen, W. M., and Xavier, A. V. (1998) *Biochemistry* **37,** 12160–12165
14. Salgueiro, C. A., da Costa, P. N., Turner, D. L., Messias, A. C., van Dongen, W. M., Saraiva, L. M., and Xavier, A. V. (2001) *Biochemistry* **40,** 9709–9716
15. Louro, R. O., Catarino, T., LeGall, J., Turner, D. L., and Xavier, A. V. (2001) *Chembiochem.* **2,** 831–837
16. Louro, R. O., Bento, I., Matias, P. M., Catarino, T., Baptista, A. M., Soares, C. M., Carrondo, M. A., Turner, D. L., and Xavier, A. V. (2001) *J. Biol. Chem.* **276,** 44044–44051
17. Louro, R. O., Catarino, T., Turner, D. L., Picarra-Pereira, M. A., Pacheco, I., LeGall, J., and Xavier, A. V. (1998) *Biochemistry* **37,** 15808–15815
18. Genthner, B. R. S., Friedman, S. D., and Devereux, R. (1997) *Int. J. Syst. Bacteriol.* **47,** 889–892
19. Miller, J. D. A., and Saleh, A. M. (1964) *J. Gen. Microbiol.* **37,** 419–423
20. Shaposhnikov, V. V., Kondratieva, E. N., and Fedorov, V. D. (1960) *Nature* **187,** 167–168
21. Pfennig, N., and Biebl, H. (1976) *Arch. Microbiol.* **110,** 3–12
22. Czjzek, M., Payan, F., Guerlesquin, F., Bruschi, M., and Haser, R. (1994) *J. Mol. Biol.* **243,** 653–667
23. Frey, M., Haser, R., Pierrot, M., Bruschi, M., and Le Gall, J. (1976) *J. Mol. Biol.* **104,** 741–743
24. Otwinowski, Z. (1993) in *Data Collection and Processing* (Sawyer, L., Isaacs, N. W., and Bailey, S., eds) pp. 71–79, Daresbury Laboratory, Warrington, UK
25. CCP4 (1994) *Acta Crystallogr. Sect. D Biol. Crystallogr.* **50,** 760–763
26. Navaza, J. (1994) *Acta Cryst. Sect. A* **50,** 157–163
27. Brünger, A. T. (1992) *X-plor: A System for Protein Crystallography and NMR,* Version 3.1, Yale University Press, New Haven
28. Sheldrick, G. M., and Schneider, T. R. (1997) *Methods Enzymol.* **277,** 319–343
29. Brünger, A. T. (1992) *Nature* **355,** 472–475
30. Roussel, A., Fontecilla-Camps, J. C., and Cambilllau, C. (1990) *XV IUCr Congress* (Authier, A., ed) pp. C66–C67, Bordeaux, France
31. Coutinho, I. B., Turner, D. L., LeGall, J., and Xavier, A. V. (1993) *Biochem. J.* **294,** 899–908
32. Murshudov, G. N., Vagin, A. A., and Dodson, E. J. (1997) *Acta Crystallogr. Sect. D Biol. Crystallogr.* **53,** 240–255
33. Ausubel, F. M., Brent, R., Kingston, R. E., Moore, D. D., Seidman, J. G., Smith, J. A., and Struhl, K. (1999) *Current Protocols in Molecular Biology* (Ausubel, F. M., Brent, R., Kingston, R. E., Moore, D. D., Seidman, J. G., Smith, J. A., and Struhl, K., eds) John Wiley & Sons, Inc, New York
34. Delgado, R., Frausto da Silva, J. J. R., Amorim, M. T. S., Cabral, M. F., Chaves, S., and Costa, J. (1991) *Anal. Chim. Acta* **245,** 271–282
35. Salgueiro, C. A., Turner, D. L., Santos, H., LeGall, J., and Xavier, A. V. (1992) *FEBS Lett.* **314,** 155–158
36. Dutton, P. L. (1978) *Methods Enzymol.* **54,** 411–435
37. Catarino, T. (1998) *Thermodynamic and Kinetic Modelling of the Redox Properties of Tetrahaem Cytochromes c3.* Ph.D. thesis, Universidade Nova de Lisboa
38. McKenna, C. E., Gutheil, W. G., and Song, W. (1991) *Biochim. Biophys. Acta* **1075,** 109–117
39. Dixon, M. (1971) *Biochim. Biophys. Acta* **226,** 241–258
40. Salgueiro, C. A., Turner, D. L., and Xavier, A. V. (1997) *Eur. J. Biochem.* **244,** 721–734
41. Turner, D. L., Brennan, L., Chamberlin, S. G., Louro, R. O., and Xavier, A. V. (1998) *Eur. Biophys. J.* **27,** 367–375
42. Louro, R. O., Correia, I. J., Brennan, L., Coutinho, I. B., Turner, D. L., and Xavier, A. V. (1998) *J. Am. Chem. Soc.* **120,** 13240–13247
43. Turner, D. L., Salgueiro, C. A., Catarino, T., LeGall, J., and Xavier, A. V. (1994) *Biochim. Biophys. Acta* **1187,** 232–235
44. Catarino, T., and Turner, D. L. (2001) *ChemBioChem.* **2,** 416–424
45. Marcus, R. A., and Sutin, N. (1985) *Biochim. Biophys. Acta* **811,** 265–322
46. Neta, P., Huie, R. E., and Harriman, A. (1987) *J. Phys. Chem.* **91,** 1606–1611
47. Christiansen, H. E. M., Coutinho, I., Conrad, L. S., Hammerstad-Pedersen, J. M., Iversen, G., Jensen, M. H., Karlsson, J. J., Ulstrup, J., and Xavier, A. V. (1994) *J. Photochem. Photobiol.* **82,** 103–115
48. Tickle, I. J., Laskowski, R. A., and Moss, D. S. (1998) *Acta Crystallogr. Sect. D Biol. Crystallogr.* **54,** 547–557
49. Morris, A. L., MacArthur, M. W., Hutchinson, E. G., and Thornton, J. M. (1992) *Proteins* **12,** 345–364
50. Ramachandran, G. N., and Sasisekharan, V. (1968) *Adv. Protein Chem.* **23,** 283–438
51. Cruickshank, D. W. J. (1996) in *Proceedings of Collaborative Computational Project 4 Study Weekend* (Dodson, E., Moore, M., Ralph, A., and Bailey, S., eds) pp. 11–22, Daresbury
52. Lee, B., and Richards, F. M. (1971) *J. Mol. Biol.* **55,** 379–400
53. Coutinho, I. B., Turner, D. L., Legall, J., and Xavier, A. V. (1995) *Eur. J. Biochem.* **230,** 1007–1013
54. Gayda, J. P., Benosman, H., Bertrand, P., More, C., and Asso, M. (1988) *Eur. J. Biochem.* **177,** 199–206
55. Moura, I., Teixeira, M., Huynh, B. H., LeGall, J., and Moura, J. J. (1988) *Eur. J. Biochem.* **176,** 365–369
56. Correia, I. J., Paquete, C. M., Louro, R. O., Catarino, T., Turner, D. L., and Xavier, A. V. (2002) *Eur. J. Biochem.* **269,** 5722–5730
57. Coletta, M., Catarino, T., LeGall, J., and Xavier, A. V. (1991) *Eur. J. Biochem.* **202,** 1101–1106
58. Capeillère-Blandin, C., Guerlesquin, F., and Bruschi, M. (1986) *Biochim. Biophys. Acta* **848,** 279–293
59. Park, J. S., Ohmura, T., Kano, K., Sagara, T., Niki, K., Kyogoku, Y., and Akutsu, H. (1996) *Biochim. Biophys. Acta* **1293,** 45–54
60. Louro, R. O., Catarino, T., Paquete, C. M., and Turner, D. L. (2004) *FEBS Lett.* **576,** 77–80
61. Xavier, A. V. (2002) *FEBS Lett.* **532,** 261–266
62. Xavier, A. V. (2004) *Biochim. Biophys. Acta* **1658,** 23–30
63. Louro, R. O. (1998) *Proton-thrusters: Energy Transduction Performed by Tetrahaem Cytochromes c3 and Its Physiological Relevance.* Ph.D. thesis, Universidade Nova de Lisboa
64. Matias, P. M., Soares, C. M., Saraiva, L. M., Coelho, R., Morais, J., Le Gall, J., and Carrondo, M. A. (2001) *J. Biol. Inorg. Chem.* **6,** 63–81
65. Louro, R. O., Catarino, T., Salgueiro, C. A., LeGall, J., and Xavier, A. V. (1996) *J. Biol. Inorg. Chem.* **1,** 34–38